Hypoxia Sensing in Resident Cardiac Macrophages Regulates Monocyte-Derived Macrophage Fate Specification following Myocardial Infarction

Farid F. Kadyrov[1], Andrew L. Koenig[1], Junedh M. Amrute[1], Wenjun Li[2], Lulu Lai[1], Carla J. Weinheimer[1], Jessica M. Nigro[1], Attila Kovacs[1], Andrea L. Bredemeyer[1], Daniel Kreisel[2,3], and Kory J. Lavine[1,3,4,*]

[1]*Cardiovascular Division, Department of Medicine, Washington University School of Medicine, St. Louis, Missouri, USA.*

[2]*Department of Surgery, Washington University School of Medicine, Saint Louis, Missouri, USA.*

[3]*Department of Pathology and Immunology, Washington University School of Medicine, Saint Louis, Missouri, USA.*

[4]*Department of Developmental Biology, Washington University School of Medicine, Saint Louis, Missouri, USA.*

***Corresponding Author**:

Kory J. Lavine, MD, PhD,
Affiliation: Division of Cardiology, Department of Medicine, Washington University School of Medicine.
Address: 660 S Euclid, Campus Box 8086, St. Louis, MO 63110.
Telephone: 314-362-1171
Email: klavine@wustl.edu

Abstract

Cardiac macrophages orchestrate inflammatory responses following myocardial injury and represent powerful determinants of cardiac tissue remodeling and outcomes. Following myocardial infarction, large numbers of monocytes are recruited to the heart, infiltrate into the myocardium, and differentiate into diverse populations of macrophages and dendritic cells with divergent inflammatory and reparative transcriptional signatures. The molecular mechanisms that drive monocyte fate decisions in the injured heart remained to be defined. Here, we tested the hypothesis that macrophage hypoxia sensing regulates monocyte differentiation and cardiac remodeling following myocardial infarction. Using a mouse model of ischemia reperfusion injury, we uncovered that deletion of the hypoxia sensor, *Hif1α*, in macrophages resulted in increased infarct size and accelerated adverse remodeling without impacting coronary angiogenesis. Single cell RNA sequencing revealed that loss of macrophage hypoxia sensing led to an overrepresentation of a subpopulation of monocyte-derived macrophages marked by Arginase 1 (*Arg*1) mRNA and protein expression. Trajectory and pathway enrichment analysis predicted that Arg1^{+} macrophages were derived from Ly6C^{hi} monocytes and represented an early stage of macrophage differentiation and expressed genes associated with metabolism and inflammation. Conditional deletion of *Hif1α* in cardiac resident macrophages and not monocyte-derived macrophages resulted in increased Arg1^{+} macrophage abundance and was sufficient to increase infarct size and accelerate adverse remodeling. Collectively, these findings identify hypoxia sensing in resident cardiac macrophages as a non-cell autonomous mediator of monocyte fate specification and outcomes in the context of myocardial infarction.

Introduction

Myocardial infarction (MI) is an ischemic event that occurs in response to cessation of coronary perfusion and initiates adverse left ventricular (LV) remodeling, which is central to the pathogenesis of heart failure (1). While numerous effective medications including β-blockers, angiotensin II receptor blockers, neprilysin inhibitors, and aldosterone antagonists are routinely used in clinical practice, heart failure continues to be a major problem that carries high morbidity and mortality rates, affecting over 23 million people worldwide with a 5-year survival rate of approximately 50% (2, 3, 4).

MI results in cardiac inflammation as a consequence of activating innate immune responses (5). Macrophages, phagocytotic members of the innate immune system, represent the primary immune cell found in the heart under steady state conditions. Cardiac macrophages are complex arising from multiple development lineages. The mouse and human heart contain two functionally distinct resident macrophage populations that can be distinguished based on C-C chemokine receptor 2 (CCR2) expression: embryonic derived $CCR2^-$ macrophages that promote tissue repair and suppress inflammation, and monocyte-derived $CCR2^+$ macrophages that initiate inflammatory responses (10, 11, 22, 53). Following MI, large numbers of pro-inflammatory $Ly6C^{hi}CCR2^+$ monocytes are recruited to the heart where they differentiate into pro-inflammatory populations of macrophages (6, 7).

Prior studies have elucidated that manipulating resident cardiac macrophage composition and interfering with monocyte recruitment has dramatic impacts on outcomes following MI (8, 9, 10, 11, 12). For example, depletion of $CCR2^+$ macrophages residing within the heart prior to MI is sufficient to reduce neutrophil infiltration, monocyte recruitment, myocardial chemokine and cytokine production, and preserve LV systolic function. Conversely, removing $CCR2^-$ cardiac macrophages leads to increased peripheral leukocyte recruitment, accelerated LV remodeling, and reductions in LV systolic function. Additionally, inhibition of monocyte recruitment has beneficial effects in mouse models of MI (9, 10, 12, 34, 46).

Recent single cell RNA sequencing studies have indicated that monocytes recruited to the injured heart differentiate into multiple distinct macrophage and dendritic cell subsets with unique gene expression signatures and localizations within the infarcted myocardium (10). The mechanistic basis by which monocytes are specified to differentiate into these populations is unknown. We hypothesized that environmental cues present within the infarcted heart instruct monocyte fate decisions. Such environmental cues may either act directly on infiltrating monocytes or indirectly through non-cell autonomous mechanisms. The latter possibility is supported by the observation that depletion of cardiac resident macrophages prior to MI is sufficient to alter the relative abundance of various monocyte-derived macrophage subsets (10).

Here, we explored hypoxia sensing as an environmental cue that may influence monocyte fate specification following MI. Hypoxia inducible factor-1 is a transcription factor consisting of the subunits HIF1α and HIF1β which regulates the transcriptional response to hypoxia (13, 14, 15). We conditionally deleted *Hif1a* in monocytes and macrophages and interrogated the functional impact of hypoxia sensing on monocyte fate specification and LV remodeling in a clinically relevant mouse model of MI (closed-chest ischemia reperfusion injury). We demonstrate that *Hif1a* deletion specifically in monocytes and macrophages increases infarct size, accelerates LV remodeling, and reduces cardiac function. Single cell RNA sequencing revealed that *Hif1a* deletion in monocytes and macrophages led to an expansion of a subpopulation of monocyte-derived macrophages marked by Arginase 1 (*Arg1*) expression and characterized by a metabolically active and inflammatory phenotype. Trajectory analysis, monocyte lineage tracing, and 2-photon intravital imaging, indicated that Arg1$^+$ macrophages represented a population that was specified early after monocyte recruitment to the infarcted heart. Deletion of *Hif1a* specifically in either resident cardiac macrophages or recruited monocytes indicated that the observed expansion of Arg1$^+$ macrophages is due to non-cell autonomous effects of defective hypoxia sensing in resident cardiac macrophages. These findings identify hypoxia sensing in resident cardiac macrophages

as a non-cell autonomous mediator of monocyte fate specification and provide evidence that monocyte fate specification is an important contributor to outcomes following MI.

Materials and Methods

Animal Models

Mus musculus were housed in ultraclean rodent barrier facility with veterinarians from the Washington University Division of Comparative Medicine on call or on site for animal care. All procedures were performed in accordance with IUCAC protocols. Strains used were Cx3cr1^{creERT2} (16) (JAX stock #020940), Hif1a$^{flox/flox}$ (17) (JAX stock #007561), Rosa26$^{flox\text{-}stop\text{-}flox\ tdTomato}$ (18) (JAX stock #007914), CCR2^{creERT2} (19), and Arg1^{YFP} (20) (JAX stock #015857) on the C57BL/6 background. Experiments were performed on mice 6-12 weeks of age. Equal numbers of male and female mice were used for experiments. For Cre recombination in all monocytes and macrophages, Cx3cr1^{creERT2} Hif1a$^{flox/flox}$ Rosa26$^{flox\text{-}stop\text{-}flox\ tdTomato}$ mice (macHif1a KO) were given tamoxifen food pellets (Envigo TD.130857) for the entirety of the MI experiment. For Cre recombination in recruited monocytes and macrophages, CCR2^{creERT2} Hif1a$^{flox/flox}$ Rosa26$^{flox\text{-}stop\text{-}flox\ tdTomato}$ mice (monoHif1a KO or monotdT) were given a single IP injection of 60 mg/kg of tamoxifen (Millipore Sigma T5648) 24 hours prior to MI. For Cre recombination of resident cardiac macrophages, Cx3cr1^{creERT2} Hif1a$^{flox/flox}$ Rosa26$^{flox\text{-}stop\text{-}flox\ tdTomato}$ mice (resHif1a KO) were given 5 daily consecutive IP injections of 60 mg/kg of tamoxifen immediately after instrumentation, followed by 9 days of normal chow (no tamoxifen) prior to MI.

Closed-chest Ischemia Reperfusion Injury

Mice were anesthetized, intubated, and mechanically ventilated. The heart was exposed, and a suture placed around the proximal left coronary artery. The suture was threaded through a 1 mm piece of polyethylene tubing to serve as the arterial occlude. Each end of the suture was exteriorized through the thorax. The skin was closed, and mice were given a 2-week recovery period prior to induction of ischemia. Ischemia was induced after anesthetizing the animals. Tension was exerted on suture ends until ST-segment elevation was seen via ECG. Following 90 minutes of ischemia time, tension was released, and the skin was then closed.

Echocardiography

Mice were sedated and 2D and M-mode images were obtained in the long and short axis views 4 weeks after MI using the VisualSonics770 Echocardiography System. Left diastolic volume, left systolic volume, akinetic area, and total LV area was measured using edge detection and tracking software (VivoLab). Ejection fraction was calculated as the (left diastolic volume – left systolic volume) / left diastolic volume. Akinetic percentage was calculated as the akinetic area / total LV area.

Syngeneic Heart Transplant and 2-photon Intravital Imaging

Cardiac grafts were harvested from donor wild type mice and transplanted into the cervical position of recipient Arg1-YFP mice after 1 hour of cold ischemia. The recipient right common carotid artery and right external jugular vein were connected to the donor ascending aorta and the donor pulmonary artery. 655-nm non targeted Q dots were injected through the intravenous route into recipient mice prior to imaging. Time-lapse imaging was performed with a custom-built 2-photon microscope running ImageWarp version 2.1 acquisition software (A&B Software) (53). Mice were imaged 24 hours after syngeneic heart transplantation. Mice were anesthetized, intubated, and ventilated for imaging. The heart was fixed to imaging coverslips and imaged for a duration of 15 minutes. Imaging is terminal and mice were euthanized.

Histology

4 weeks after MI, mice were euthanized, and hearts perfused with PBS. Hearts were fixed overnight with 4% PFA in PBS at 4°C, cut into thirds on the transverse plane, placed into histology cassettes for paraffin embedding, and dehydrated in 70% ethanol in water. Hearts were paraffin embedded and cut into 4 µm sections and mounted on positively charged slides. Tissues were stained by Gomori's Trichrome staining (Richard-Allan Scientific 87020) and WGA staining (Vector Laboratories RL-1022). Trichrome staining was imaged using a Meyer PathScan Enabler IV. Measurement of infarct length and LV length was performed in FIJI, with data quantification normalizing the length of the infarct to the length of the LV (52). WGA

staining was imaged using the 20x objective of a Zeiss LSM 700 confocal microscope. 4-5 20x fields of the border zone of the infarct were taken per mouse. 12 cross sectional (not longitudinal) cardiomyocytes per 20x field were selected at random. Measurement of cross-sectional cardiomyocyte area was performed in FIJI. Data is displayed as the average cardiomyocyte cross sectional area per mouse.

4 days after MI, mice were euthanized, and hearts perfused with PBS. Hearts were incubated in 2% 2, 3, 5-triphenyltetrazolium chloride (Millipore Sigma T8877) in PBS for 30 minutes at 37°C and then washed in 4% PFA in PBS for 24 hours at 4°C. Pictures were taken with a ZEISS SteREO Discovery.V12 Stereo Microscope. Quantification of total infarct area normalized to total heart area was performed with FIJI.

Immunofluorescence

4 days after MI, mice were euthanized, and hearts perfused with PBS. Hearts were cut midway on the transverse plane and fixed overnight with 4% PFA in PBS at 4°C. They were then dehydrated in 30% sucrose in PBS overnight at 4°C. Hearts were embedded in O.C.T. (Sakura 4583) and frozen at -80°C for 30 minutes. Hearts were then sectioned at 15 µm using a Leica Cryostat, mounted on positively charged slides, and stored at -80°C. For staining, the following steps were performed at room temperature and protected from light. Slides were brought to room temperature for 5 minutes and washed in PBS for 5 minutes. Sections were then permeabilized in 0.25% Triton X in PBS for 5 minutes. Sections were then blocked in 5% BSA in PBS for 1 hour. Sections were then stained with primary antibody diluted in 1% BSA in PBS for 1 hour (rat anti CD34 abcam ab8158 1:200 dilution, rat anti CD68 BioLegend 137002 1:400 dilution, rat anti Ly6g BD Pharmingen 551459 1:100 dilution, rabbit anti Arg1 Cell Signaling Technology 93668 1:100 dilution). Sections were then washed 3 times 5 minutes each with PBS-Tween. After washing, the appropriate secondary antibodies were added diluted in 1% BSA in PBS for 1 hour at a 1:1000 dilution (Goat anti Rat 488 Life Technologies a11006, Goat anti Rat 647 a21247 Life Technologies a21247, or Donkey anti Rabbit 647 Abcam ab150075). Slides were again washed 3 times 5 minutes each with PBS-T,

and then mounted with DAPI mounting media (Millipore Sigma F6057) and cover slipped. Slides were stored at 4°C protected from light and imaged within 1 week. For immunofluorescence staining of paraffin embedded tissues collected 4 weeks after MI, the OPAL 4-Color Manual IHC Kit (Akoya Biosciences NEL810001KT) was used. Primary antibodies used were: Anti CD34 (abcam ab8158 1:200 dilution), anti a-SMA (Invitrogen 14-9760-82 1:500 dilution).

Slides were imaged using the 20x objective of a Zeiss LSM 700 confocal microscope. Visualization of tdTomato was from the endogenous signal. For quantification, 5 20x fields of either the border zone (CD34, aSMA) or infarct zone (CD68, Ly6g, Arg1) were taken per mouse. Quantification of cell numbers, area percentages, or a-SMA+ vessels were performed in FIJI, and data is displayed as the average of each 20x field per mouse.

Flow Cytometry

Hearts were perfused with PBS, weighed, minced, and digested for 45 minutes at 37°C in DMEM (Gibco 11965-084) containing 4500 U/ml Collagenase IV (Millipore Sigma C5138), 2400 U/ml Hyaluronidase I (Millipore Sigma H3506), and 6000 U/ml DNAse I (Millipore Sigma D4527). Enzymes were deactivated with HBSS containing 2% FBS and 0.2% BSA and filtered through 40-micron strainers. Cells were incubated with ACK lysis buffer (Gibco A10492-01) for 5 minutes at room temperature. Cells were washed with DMEM and resuspended in 100 µl of FACS buffer (PBS containing 2% FBS and 2mM EDTA). Cells were incubated in a 1:200 dilution of fluorescence conjugated monoclonal antibodies for 30 minutes at 4°C. Samples were washed in FACS buffer and resuspended in a final volume of 250 µl FACS buffer. Flow cytometry and sorting was performed using a BD FACS melody. For intravascular staining of CD45, 200 µl of CD45 APC (BioLegend 103112) was injected intravascularly at a concentration of 5µg/ml in PBS 5 minutes prior to tissue collection. Hearts were then perfused with 10 ml of PBS. For intracellular staining of Arg1-YFP, the BioLegend Cyto-Fast Fix/Perm Buffer Set (BioLegend 426803) was used following staining for surface markers, and intracellular staining with GFP-PE (BioLegend 338003) was performed. For FACS analysis of

monocytes, neutrophils, and macrophages in macHif1a KO mice, antibodies used were: CD45 percp/cy5.5 (BioLegend 103132), CD64 PE/CY7 (BioLegend 139313), LY6G FITC (BioLegend 127606), and LY6C APC (BioLegend 128016). For sorting of monocytes and macrophages in macHif1a KO mice for single cell RNA sequencing, antibodies used were: CD45 percp/cy5.5(BioLegend 103132), Ly6g FITC (BioLegend 127606), Ly6c APC (BioLegend 128016), DAPI (BV421) (BD Pharmingen 564907), and CD64 PE/Cy7 (BioLegend 139313).For FACS analysis of intravascular Arg1-YFP macrophages, antibodies used were: CD45 percp/cy5.5(BioLegend 103132), CD45 APC (BioLegend 103112), Ly6c bv510 (BioLegend 128033), CD11b bv421 (BioLegend 101235), ly6g apc/cy7 (BioLegend 127623), CD64 pe/cy7 (BioLegend 139313), and GFP-PE (BioLegend 338003).

Single Cell RNA Sequencing Analysis

Monocytes and macrophages from macHif1a KO and control mice were sorted 5 days after MI. Single cell RNA sequencing libraries were generated using the 10X Genomics 5'v1 platform. 10,000 cells per library were inputted for first strand synthesis. Second strand synthesis used 14 cycles of PCR amplification. Libraries were constructed using the 10x Genomics 5'v1 GEM protocol and libraries were sequenced using a NovaSeq 6000 at the McDonnel Genome Institute. Sequencing reads were aligned to the GRcm38 transcriptome using CellRanger (v3.1.0) from 10X Genomics. Downstream data processing was performed in the R package Seurat v4 (21). SCtransform was used to scale and normalize the data for RNA counts. Quality control filters of 500-5000 genes/cell, less than 10% mitochondrial reads/cell, and less than 20,000 read counts/cell were applied. The number of PCAs used was selected based on elbow plots, data was clustered at multiple resolutions using highly variable genes, and UMAP projections were generated for data visualization. Contaminating populations of stroma, nk cells, t cells, cardiomyocytes, neutrophils, and b cells were excluded from analysis. Annotation of cell populations was achieved by using label transfer in Seurat, mapping the data to a reference data set of myeloid cells present in the mouse heart 3, 7, 13, and 28 days after MI (Koenig et al.-in preparation, 23). Differential gene expression between macHif1a KO

and control mice was performed through Seurat using DEseq2 (24). Genes with a log2FC > 0.1 or < -0.1 and adjusted p value of < 0.05 were used as input for WikiPathways 2019 Mouse analysis in EnrichR (25, 26, 27, 28). The top 30 genes upregulated in macHif1a KO ('Spp1', 'Fn1', 'Xist', 'S100a4', 'Crip1', 'S100a6', 'Lgals3', 'Ccl9', 'Plin2', 'Ccl6', 'Cd9', 'S100a10', 'Capg', 'Anxa1', 'Gpnmb', 'Prdx1', 'Vim', 'Ctsl', 'Fabp5', 'Acp5', 'Anxa2', 'Ifitm3', 'Ifi30', 'Lpl', 'Txn1', 'Arg1', 'Ly6a', 'Tmsb10', 'Rhoc', 'Lmna') was used to plot a Z-score of differentially expressed genes on the UMAP. Differential gene expression of upregulated genes in each subpopulation was generated in Seurat using FindAllMarkers with a minimum fraction (min.pct) of 0.1 and a logFC threshold of 0.1. Genes with a log2FC > 0.1 and adjusted p value of < 0.05 within the Arg1 population were used as input for Wikipathways 2019 Mouse analysis and ChEA 2016 transcription factor analysis in EnrichR (25, 26, 27, 28, 29).

Palantir Trajectory Analysis

The Palantir Python package was used for trajectory analysis (30). Prior to inputting data to Palantir, the resident macrophage subpopulation was removed from the Seurat object and cell cycle regression was performed using Seurat. Monocytes were used as the starting cell type for Palantir. Highly variable gene analysis was not used. The eigenvectors used was 5. The number of waypoints used was 600. The outputted pseudotime and entropy values for each cell was used to generate plots in R.

Statistical Analysis

For analysis of echocardiography, histology, immunofluorescence, and FACS, two tailed t-test assuming equal variance was performed in Excel. 4-6 replicates were used for experiments. $P < 0.05$ was *a priori* considered statistically significant. Data was plotted using Prism software.

Data Availability

Single Cell RNA sequencing data is available upon request.

Code Availability

R and Python scripts are available upon request.

Results

Deletion of *Hif1a* in monocytes and macrophages results in increased infarct size, accelerated LV remodeling, and reduced LV systolic function following MI. To assess the functional requirement for hypoxia sensing in monocytes and macrophages following MI, we subjected littermate control and *Cx3cr1*^{creERT2}*Hif1a*$^{flox/flox}$ mice to closed-chest ischemia reperfusion injury (90 minutes of ischemia) to simulate reperfused MI (16, 17). Tamoxifen chow was given throughout the entirety of the experiment to induce *Hif1a* deletion in all monocytes and macrophages (macHif1a KO) (**Figure 1A**). Echocardiography performed 4 weeks after MI revealed that macHif1a KO mice had increased akinetic left ventricular (LV) area, reduced ejection fraction, and increased LV diastolic and systolic volume compared to controls (**Figure 1B-C**). TTC staining performed within 4 days after MI showed no significant difference in initial infarct area between macHif1a KO and control mice, indicating that increased final infarct size in macHif1a KO mice is due to infarct expansion and remodeling rather than an increase in the initial extent of myocardial injury (**Figure 1D**). Trichrome and WGA staining performed 4 weeks after MI revealed increased in infarct size and cardiomyocyte hypertrophy in macHif1aKO mice compared to controls, respectively (**Figure 1E-F**).

In the context of MI and heart failure, HIF1α is thought to contribute to coronary angiogenesis and neo-vascularization of the infarct and border zone areas (31). Immunofluorescence staining for CD34 (microvasculature marker) and smooth muscle actin (α-SMA, large blood vessel marker) did not reveal any reduction in coronary vascular density in macHif1a KO hearts (**Supplementary Figure 1A-E**) (32). To access whether *Hif1a* deletion in monocytes and macrophages alter the abundance of major immune cell populations that infiltrate the heart after MI (33), we performed immunofluorescence staining and flow cytometry analysis of macHif1a KO mice and littermate controls 4 days after MI. We observed no significant differences in the total number of monocytes, macrophages, or neutrophils within infarct and border zones between experimental groups (**Supplementary Figure 1F-K**).

***Hif1a* deletion induces a shift in monocyte fate specification following MI.** Previous single cell RNA sequencing studies have revealed that altering the identity of macrophages present within the heart following MI has profound effects on LV remodeling and function (10, 34). We hypothesized that deletion of *Hif1a* in monocytes and macrophages impacts the specification and differentiation of infiltrating monocytes following MI. To evaluate this hypothesis, we utilized single cell RNA sequencing as a tool to identify transcriptionally distinct populations of monocytes and their progeny (macrophages and dendritic cells) in control and macHif1a KO mice. Single cell RNA sequencing was performed on cardiac $CD45^+Ly6G^-Ly6C^+CD64^+DAPI^-$ cells isolated by flow cytometry on day 5 following MI (**Supplementary Figure 2A**). To annotate monocyte, macrophage, and dendritic cell populations with high confidence, single cell RNA sequencing data generated from macHif1a KO and control mice was mapped using label transfer to a reference data set of identical myeloid cells ($CD45^+Ly6G^-Ly6C^+CD64^+DAPI^-$) isolated from the mouse heart 3, 7, 14, and 28 days after MI (Koenig et al in preparation, 23). Reference mapping performance was evaluated by calculating mapping scores and plotting transcriptional signatures of reference monocyte, macrophage, and dendritic cell populations in the query dataset. Each of these metrics indicated excellent reference mapping precision (**Supplementary Figure 2B-H**).

Composition analysis of myeloid cells in control and macHif1a KO mice demonstrated a robust overrepresentation of a macrophage population marked by *Arg1* expression (population 5) in macHif1a KO hearts (**Figure 2A-D**) supporting the possibility that hypoxia sensing in monocytes and/or macrophages influences the differentiation of infiltrating monocytes. Differential gene expression analysis comparing control and macHif1a KO monocytes, macrophages, and dendritic cells revealed that many of the genes increased in macHif1a KO cells were selectively expressed by $Arg1^+$ macrophages (**Figure 2E**). Genes differentially expressed across genotypes were associated with metabolism and IFNγ signaling (**Figure 2F**). Given the increased abundance of $Arg1^+$ macrophages and mapping of differentially expressed genes to

this population, we further examined the transcriptional profile of Arg1$^+$ macrophages. Arg1$^+$ macrophages were marked by the expression of genes involved in metabolic and oxidative stress pathways (**Figure 2G**). ChEA 2016 transcription factor enrichment predicted that marker genes of Arg1$^+$ macrophages were regulated by transcription factors involved in inflammation including NCOR, NRF2, ATF3, SMRT, RELA, JUND, and BRD4 (**Figure 2H**) (35, 36, 37, 38, 39).

We next performed Palantir trajectory analysis (30) to ascertain the differential trajectory of monocytes, macrophages, and dendritic cells in control and macHif1a KO hearts. Monocytes were selected as the least differentiated cell population. Cell cycle regression was performed using Seurat to reduce the impact of cell cycle on trajectory analysis and resident macrophages were excluded since they are not part of the monocyte lineage (30, 40). Within the predicted differentiation trajectory, monocytes had the high entropy and low pseudotime values consistent with the assumption that monocytes represent the starting cell state. Intriguingly, Arg1$^+$ macrophages also displayed high entry and low pseudotime values suggesting that this cell state may represent an early event in monocyte differentiation (**Figure 2I**). These data support the concept that hypoxia sensing in monocytes and/or macrophages influences proximal steps in monocyte fate specification.

Arg1$^+$ macrophages are monocyte-derived and specified prior to myocardial extravasation. We next sought to biologically validate predictions made from our single cell RNA sequencing data. We first confirmed that Arg1$^+$ macrophage abundance is increased in the infarct zone of macHif1a KO hearts compared to controls (**Figure 3A, C**). To determine if Arg1$^+$ macrophages are monocyte derived, we utilized a monocyte fate labeling strategy. In order to specifically label monocytes and their progeny, we established a tamoxifen regimen where a single dose of 60mg/kg labels monocytes and not macrophages in *CCR2^{creERT2}Rosa26^{tdTomato}* mice (**Supplementary Figure 3**). We subjected *CCR2^{creERT2}Hif1a$^{flox/flox}$Rosa26^{tdTomato}* mice to closed chest-ischemia reperfusion injury and assessed

tdTomato expression 5 days after MI. Mice were treated with a single dose of tamoxifen (60mg/kg) 24 hours prior to MI. We observed that the overwhelming majority of Arg1$^+$ macrophages were tdTomato positive indicating that Arg1$^+$ macrophages are derived from monocytes (**Figure 3B, D**).

Palantir trajectory analysis predicted that Arg1$^+$ macrophages represented an early event in monocyte differentiation. To investigate this possibility, we performed intravital 2-photon microscopy to visualize Arg1$^+$ macrophage specification in real time. To accomplish this, we leveraged a previously established syngeneic heart transplant model of ischemia reperfusion injury (10, 20). Donor hearts were harvested, placed on ice for 60 minutes, and then transplanted into *Arg1^{YFP}* reporter in the cervical position. Donor hearts were imaged 24 hours after heart transplantation. We observed YFP$^+$ cells within the intravascular and extravascular compartments (**Figure 3E**). Intravascular YFP+ cells appeared to be crawling on the endothelium suggesting that Arg1$^+$ macrophage specification is initiated prior to extravasation into the myocardium. To verify that Arg1$^+$ macrophages are indeed present within the intravascular compartment, we employed a flow cytometry-based approach to label intravascular leukocytes. *Arg1^{YFP}* reporter mice were assayed 2 days after MI, a time point where monocytes are robustly recruited to the heart (41). A fluorescently conjugated CD45 antibody (CD45iv) was injected intravascularly into *Arg1^{YFP}* reporter mice 5 minutes prior to tissue harvest. Intravascular injection of CD45 antibodies has previously been shown to differentiate intravascular leukocytes from those within the myocardial compartment (42). Using this strategy, we detected Arg1$^+$ macrophages within both the extravascular (CD45iv-) and intravascular (CD45iv+) compartment (**Figure 3F, Supplementary Figure 4**). Furthermore, mean fluorescence intensity of Ly6c staining was higher in Arg1+ cells in the intravascular compartment in comparison to Arg1+ cells in the extravascular compartment (**Figure 3G**). Overall, the results of our Palantir trajectory analysis, lineage tracing studies, intravital 2-photon imaging, and intravascular flow cytometry strongly suggest that Arg1$^+$ macrophages are monocyte-derived and are specified early after monocyte recruitment to the infarcted heart.

Conditional deletion of *Hif1a* in cardiac resident macrophages and not monocyte-derived macrophages increases the abundance of Arg1$^+$ macrophages. To ascertain whether hypoxia sensing in recruited monocytes and/or cardiac resident macrophages contributes to the specification of Arg1$^+$ macrophages, we specifically deleted *Hif1a* in each of these populations. To delete *Hif1a* exclusively in infiltrating monocytes and their progeny, we treated *CCR2^{creERT2}Hif1a$^{flox/flox}$Rosa26^{tdTomato}* mice a single dose of tamoxifen (60mg/kg) 24 hours prior to MI (monoHif1a KO). Recombination (reported by tdTomato expression) was induced in most macrophages within the infarct. Infrequent tdTomato$^+$ macrophages were observed within the border and remote zone. To delete *Hif1a* exclusively in resident cardiac macrophages, we treated *Cx3cr1^{creERT2}Hif1a$^{flox/flox}$Rosa26^{tdTomato}* mice with tamoxifen (60 mg/kg daily for 5 days) immediately after instrumentation to label all monocytes and macrophages. Mice then received normal chow for 9 days prior to MI (resHif1a KO). During this time period monocytes are replenished from hematopoietic progenitors and only cardiac resident macrophages remain labeled (10). tdTomato$^+$ macrophages are predominately observed in the border and remote zones following MI with a low frequency of tdTomato$^+$ macrophages present within the infarct (**Supplementary Figure 5**).

To delineate whether deleting *Hif1a* in infiltrating monocytes and/or cardiac resident macrophages contributed to expansion of Arg1$^+$ macrophages, we quantified the proportion of Arg1$^+$ macrophage by immunostaining 4-5 days after MI using the above genetic strategies. Deletion of *Hif1a* in monocytes (monoHif1a KO mice) did not result in increased Arg1$^+$ macrophages within the infarct compared to controls (**Figure 4A, C**). Conversely, deletion of *Hif1a* in cardiac resident macrophages (resHif1a KO mice) was sufficient to increase the abundance of Arg1$^+$ macrophages within the infarct compared to controls (**Figure 4B, D**). This data indicates that defective hypoxia sensing in cardiac resident macrophages influences the specification of monocytes into Arg1$^+$ macrophages through a non-cell autonomous mechanism.

***Hif1a* deletion in resident cardiac macrophages contributes to adverse outcomes following MI.** We next examined whether deletion of *Hif1a* in cardiac resident macrophages (resHif1a KO mice) contributes to LV remodeling following MI. Control and resHif1a KO mice were treated with tamoxifen (60mg/kg for 5 days) immediately after instrumentation. Mice were then fed normal chow for 9 days and then subjected to MI (**Figure 5A**). Echocardiography performed 4 weeks after MI revealed that resHif1a KO mice had reduced ejection fraction, increased LV diastolic and systolic volume, and increased akinetic LV area compared to controls (**Figure 5B-D**). Trichrome staining of the fibrotic infarct performed 4 weeks after MI revealed increased infarct size in resHif1a KO mice compared to controls. WGA staining was performed to examine changes in cardiomyocyte hypertrophy. We observed a statistically insignificant trend towards increased cardiomyocyte size within the border zone in resHif1a KO mice compared to controls (**Figure 5E-F**). These findings causatively link defective hypoxia sensing in cardiac resident macrophages with adverse post-MI outcomes and indicate that deletion of *Hif1a* in resident cardiac macrophages is sufficient to recapitulate many of the phenotypes observed in mice lacking *Hif1a* in all monocytes and macrophages including increased infarct size, accelerated LV remodeling, and reduced LV systolic function.

Discussion

In this study, we showed that *Hif1a* deletion in all monocytes and macrophages (macHif1a KO mice) led to adverse outcomes following MI. Single cell RNA sequencing revealed that defective hypoxia signaling in monocytes and macrophages influenced monocyte fate specification resulting in an increase in Arg1$^+$ macrophages located within the infarct of macHif1a KO mice. Trajectory analysis, immunofluorescence, lineage tracing, intravital imaging, and flow cytometry determined that Arg1$^+$ macrophages are monocyte-derived and are specified at an early time point during monocyte to macrophage differentiation in the context of MI. Mechanistically, hypoxia sensing in infiltrating monocytes did not influence the specification of Arg1$^+$ macrophages. Instead, hypoxia sensing in cardiac resident macrophages was sufficient to increase the abundance of Arg1$^+$ macrophages and accelerate LV remodeling following MI through a non-cell autonomous mechanism.

Previous studies have investigated the role of macrophage *Hif1a* in mouse models of cardiac injury and heart failure. *LysM^{cre}Hif1a$^{flox/flox}$* mice subjected to transverse aortic constriction results in increased cardiac fibrosis and a reduction in ejection fraction (43). Interestingly, DeBerge *et al* reported that *LysM^{cre}Hif1a$^{flox/flox}$* mice display decreased infarct size and increased ejection fraction following permanent occlusion MI (44). It is possible that differences in MI models (closed-chest ischemia reperfusion injury vs. open chest permanent coronary ligation), cellular specificity, or temporal control of Cre recombinase activity account for differences in observed phenotypes. LysM^{cre} is active during development and is not specific to macrophages. Cre activity is detected throughout the myeloid compartment including neutrophils (44, 45).

Consistent with previous studies, we found that deletion of *Hif1a* in monocytes and macrophages did not influence total macrophage numbers in response to sterile inflammation (44, 47). However, single cell RNA sequencing revealed that *Hif1a* in monocytes and macrophages influenced monocyte fate specification after MI. A population of monocyte-derived macrophages marked by Arg1 was markedly

overrepresented in macHif1a KO mice after MI compared to controls. While the exact functions of Arg1$^+$ macrophages remained to be defined, pathway analysis and transcription factor enrichment suggested that Arg1$^+$ macrophages are metabolically active and pro-inflammatory. These findings contrast with prior literature arguing that Arg1 is a marker of the M2 macrophage phenotype (48, 49, 50). However, the relevance of the M1/M2 paradigm in the context of MI is uncertain (51). Further studies are required to clarify the functions of Arg1$^+$ macrophages following MI.

Palantir trajectory analysis predicted that Arg1$^+$ macrophages are monocyte-derived and specified early during monocyte to macrophage differentiation. Our lineage tracing, intravital imaging, and flow cytometry data confirmed that Arg1$^+$ macrophages are derived from monocytes and provide evidence that Arg1$^+$ macrophages are specified prior to monocyte infiltration into the myocardium. These provocative data suggest that monocyte fate decisions may be initiated within the vascular compartment. Trajectory analysis also predicted that Arg1$^+$ macrophages may represent an intermediate cell fate that gives rise to more mature macrophage populations. The possibility that transitional macrophage subsets contribute to myocardial inflammation and remodeling is intriguing and will need to be examined using specific lineage tracing methodologies.

We observed that deletion of *Hif1a* in monocytes did not influence the specification of Arg1$^+$ macrophages. Instead, *Hif1a* deletion in cardiac resident macrophages was sufficient to increase the abundance of Arg1$^+$ macrophages within the infarct. This data indicates that aberrant hypoxia sensing in resident cardiac macrophages has a non-cell autonomous effect on monocyte specification. This finding mirrors the observation that depletion of CCR2$^-$ cardiac resident macrophages prior to MI results in increased Arg1$^+$ macrophages within the infarct (10). It is possible that *Hif1a* deletion impacts the survival or cell signaling properties of cardiac resident macrophages during MI. Cardiac resident macrophage death represents an important event following myocardial infarction that may impact outcomes (34).

Additional studies are required to determine how defective hypoxia signaling impacts the survival and signaling properties of cardiac resident macrophages.

In conclusion, we demonstrate that hypoxia sensing in cardiac resident macrophages has a protective role following myocardial infarction through modulation of monocyte fate decisions. Defective hypoxia sensing resulted in increased abundance of a population of Arg1^{+} macrophages predicted to represent an inflammatory intermediate of monocyte differentiation that is specified prior to myocardial extravasation. Collectively, our findings provide new insights into the complexity of monocyte fate specification and signify that monocyte differentiation is an important contributor to outcomes following MI.

Figure 1:

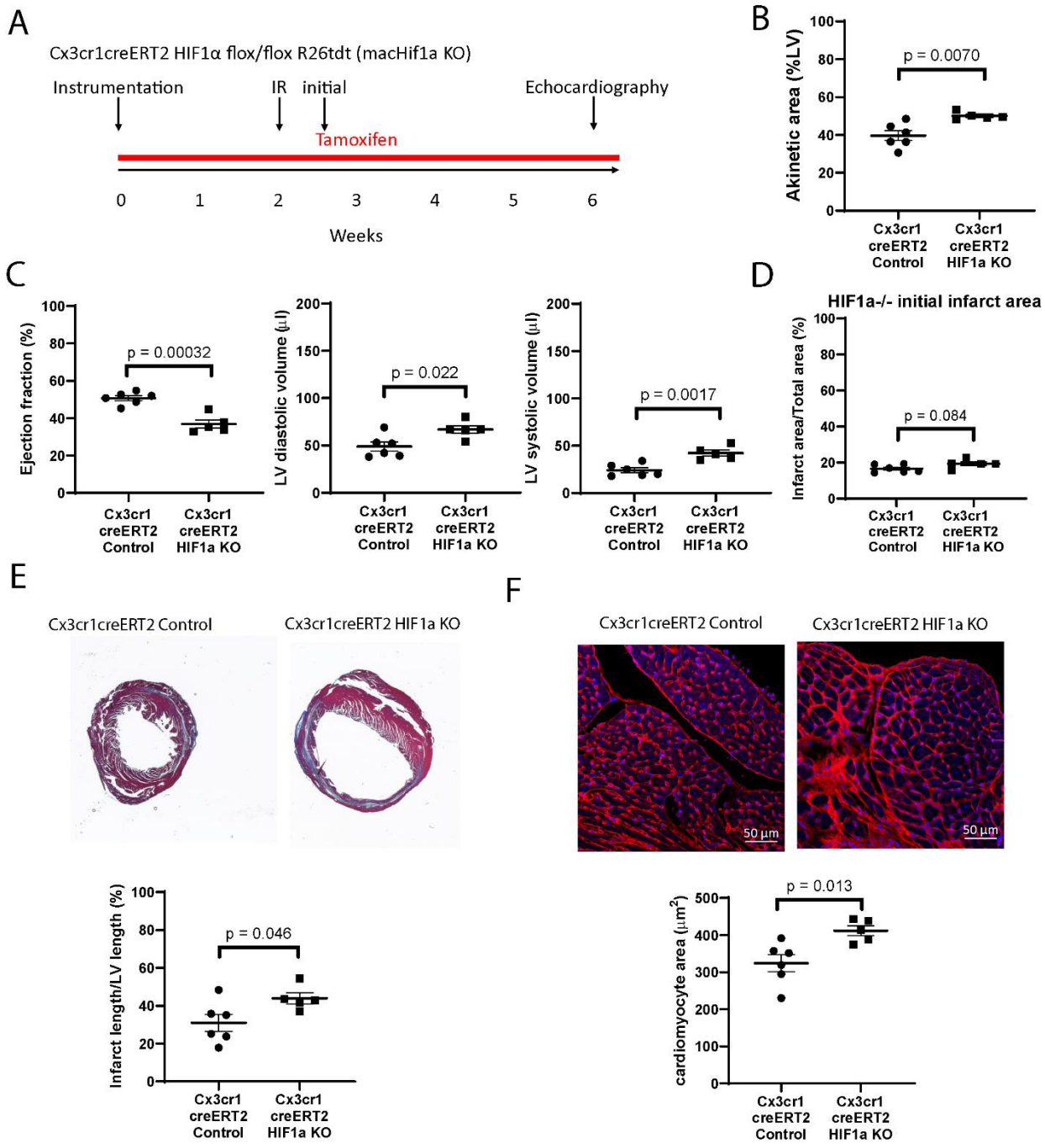
A
Cx3cr1creERT2 HIF1α flox/flox R26tdt (macHif1a KO)
Instrumentation
IR
initial
Echocardiography
Tamoxifen
0
1
2
3
4
5
6
Weeks
B
Akinetic area (%LV)
p = 0.0070
Cx3cr1 creERT2 Control
Cx3cr1 creERT2 HIF1a KO
C
Ejection fraction (%)
p = 0.00032
LV diastolic volume (µl)
p = 0.022
LV systolic volume (µl)
p = 0.0017
D
HIF1a-/- initial infarct area
Infarct area/Total area (%)
p = 0.084
E
Cx3cr1creERT2 Control
Cx3cr1creERT2 HIF1a KO
Infarct length/LV length (%)
p = 0.046
F
Cx3cr1creERT2 Control
Cx3cr1creERT2 HIF1a KO
50 µm
50 µm
cardiomyocyte area (µm²)
p = 0.013

Figure 1: *Hif1a* deletion in monocytes and macrophages leads to accelerated LV remodeling and reduced cardiac function after MI. A.) Experimental outline of ischemia reperfusion injury in *Cx3cr1*^{creERT2}*Hif1a*$^{flox/flox}$ mice. Tamoxifen chow was given throughout the course of the experiment. Closed chest IRI was performed 2 weeks after instrumentation, and echocardiography was performed 4 weeks after MI. Tissues were collected 4 days and 4 weeks after MI for analysis. B.) Echocardiography quantification 4 weeks after MI of akinetic area as a percentage of the left ventricle between *Hif1a* KO and Control mice. C.) Echocardiography quantification 4 weeks after MI of ejection fraction, left ventricular diastolic volume, and left ventricular systolic volume between *Hif1*a KO and Control mice. D.) Quantification of TTC staining 4 days after MI to determine initial infarct area between *Hif1a* KO and Control mice. E.) Trichrome staining and quantification of *Hif1*a KO and Control hearts 4 weeks after MI. Data is displayed as the length of the infarct in blue as a percentage of the total length of the left ventricle. F.) WGA staining of the border zone of the infarct 4 weeks after MI and quantification of the average cardiomyocyte area in *Hif1a* KO and Control hearts. Data points represent the average of 5 20x fields per mouse, with 12 cardiomyocytes selected at random per 20x field. P-values are determined using a two tailed t-test assuming equal variance.

Figure 2:

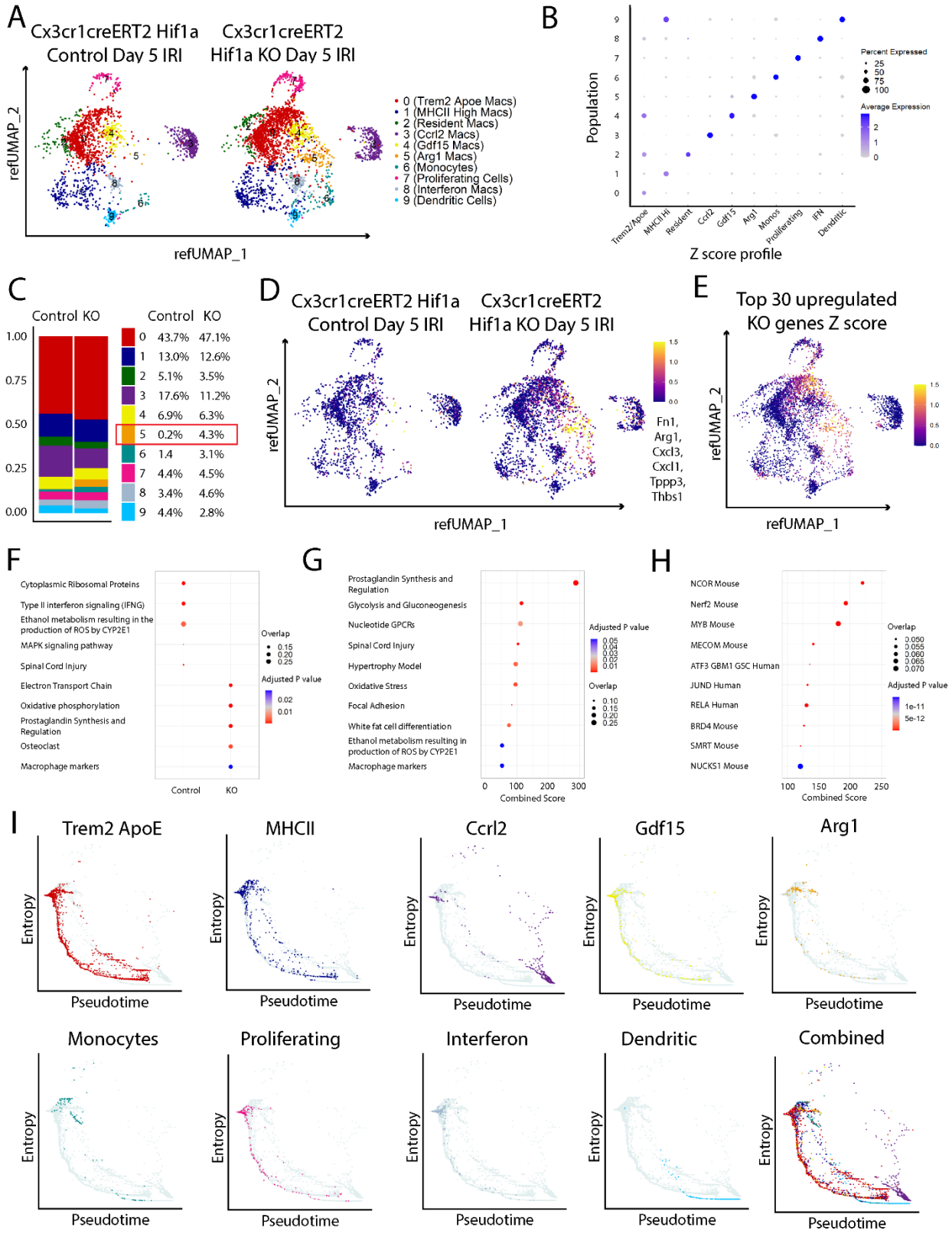
A
Cx3cr1creERT2 Hif1a Control Day 5 IRI
Cx3cr1creERT2 Hif1a KO Day 5 IRI
refUMAP_2
refUMAP_1
0 (Trem2 Apoe Macs)
1 (MHCII High Macs)
2 (Resident Macs)
3 (Ccrl2 Macs)
4 (Gdf15 Macs)
5 (Arg1 Macs)
6 (Monocytes)
7 (Proliferating Cells)
8 (Interferon Macs)
9 (Dendritic Cells)
B
Population
Percent Expressed
Average Expression
Trem2/Apoe
MHCII Hi
Resident
Ccrl2
Gdf15
Arg1
Monos
Proliferating
IFN
Dendritic
Z score profile
C
Control KO
Control KO
0 43.7% 47.1%
1 13.0% 12.6%
2 5.1% 3.5%
3 17.6% 11.2%
4 6.9% 6.3%
5 0.2% 4.3%
6 1.4 3.1%
7 4.4% 4.5%
8 3.4% 4.6%
9 4.4% 2.8%
D
Cx3cr1creERT2 Hif1a Control Day 5 IRI
Cx3cr1creERT2 Hif1a KO Day 5 IRI
refUMAP_2
refUMAP_1
Fn1, Arg1, Cxcl3, Cxcl1, Tppp3, Thbs1
E
Top 30 upregulated KO genes Z score
refUMAP_2
refUMAP_1
F
Cytoplasmic Ribosomal Proteins
Type II interferon signaling (IFNG)
Ethanol metabolism resulting in the production of ROS by CYP2E1
MAPK signaling pathway
Spinal Cord Injury
Electron Transport Chain
Oxidative phosphorylation
Prostaglandin Synthesis and Regulation
Osteoclast
Macrophage markers
Control
KO
Overlap
Adjusted P value
G
Prostaglandin Synthesis and Regulation
Glycolysis and Gluconeogenesis
Nucleotide GPCRs
Spinal Cord Injury
Hypertrophy Model
Oxidative Stress
Focal Adhesion
White fat cell differentiation
Ethanol metabolism resulting in production of ROS by CYP2E1
Macrophage markers
Adjusted P value
Overlap
Combined Score
H
NCOR Mouse
Nerf2 Mouse
MYB Mouse
MECOM Mouse
ATF3 GBM1 GSC Human
JUND Human
RELA Human
BRD4 Mouse
SMRT Mouse
NUCKS1 Mouse
Overlap
Adjusted P value
Combined Score
I
Trem2 ApoE
MHCII
Ccrl2
Gdf15
Arg1
Monocytes
Proliferating
Interferon
Dendritic
Combined
Entropy
Pseudotime

Figure 2: Single cell RNA sequencing of monocytes, macrophages, and dendritic cells 5 days after MI reveals overrepresentation of Arg1$^+$ macrophages in *Hif1a* conditional knockout mice. A.) UMAP of single cell RNA sequencing data 5 days after MI. B.) Dot plot displaying Z-scores of transcriptional signatures that mark each monocyte, macrophage, and dendritic cell population. C.) Stacked bar graph representing the proportion of each monocyte, macrophage, and dendritic cell population in the data set split between Control and *Hif1a* KO conditions. D.) Z-score profile of Arg1$^+$ macrophages (*Fn1, Arg1, Cxcl3, Cxcl1, Tppp3, Thbs1*) plotted on a UMAP and split between Control and *Hif1a* KO conditions. E.) Z-scores of the top 30 upregulated genes in *Hif1a* KO cells determined by differential expression analysis within Seurat plotted on a UMAP. F.) Dot plot of the top 5 upregulated pathways (Enrichr WikiPathways 2019 Mouse) in *Hif1a* KO compared to control cells. Top pathways are ordered by the combined score. G.) Dot plot of top 10 upregulated pathways (Enrichr WikiPathways 2019 Mouse) in Arg1$^+$ macrophages. Top pathways are ordered by the combined score. H.) Dot plot of the top 10 ChEA 2016 EnrichR transcription factors in Arg1$^+$ macrophages. I.) Plots of Entropy vs Pseudotime values for each monocyte, macrophage, and dendritic cell population from Palantir analysis.

Figure 3:

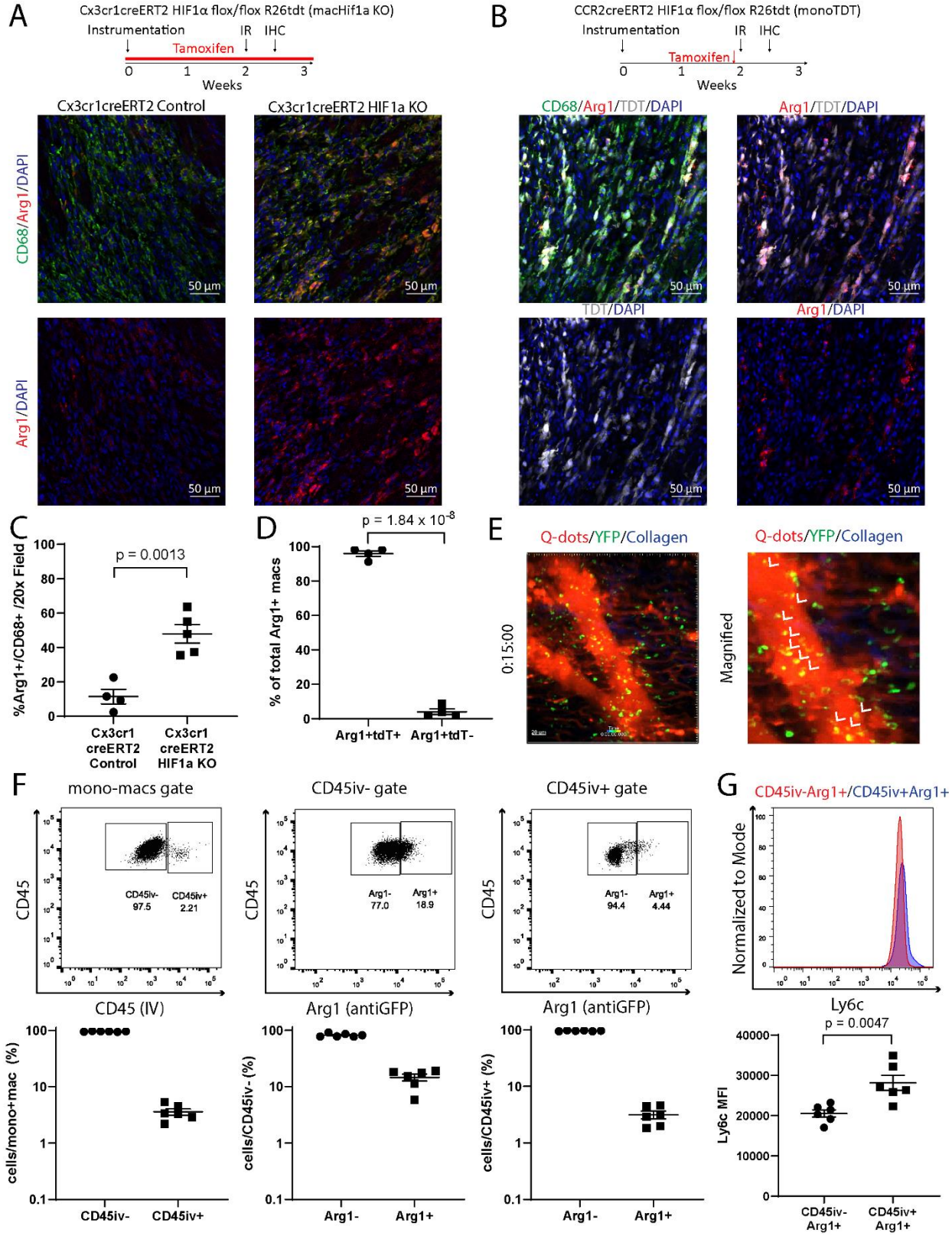
A
Cx3cr1creERT2 HIF1α flox/flox R26tdt (macHif1a KO)
Instrumentation
IR
IHC
Tamoxifen
0
1
2
3
Weeks
Cx3cr1creERT2 Control
Cx3cr1creERT2 HIF1a KO
CD68/Arg1/DAPI
Arg1/DAPI
50 µm
B
CCR2creERT2 HIF1α flox/flox R26tdt (monoTDT)
CD68/Arg1/TDT/DAPI
Arg1/TDT/DAPI
TDT/DAPI
Arg1/DAPI
C
%Arg1+/CD68+ /20x Field
p = 0.0013
Cx3cr1 creERT2 Control
Cx3cr1 creERT2 HIF1a KO
D
% of total Arg1+ macs
p = 1.84 x 10-8
Arg1+tdT+
Arg1+tdT-
E
Q-dots/YFP/Collagen
0:15:00
Magnified
F
mono-macs gate
CD45iv- gate
CD45iv+ gate
CD45
CD45iv-
97.5
CD45iv+
2.21
Arg1-
77.0
Arg1+
18.9
Arg1-
94.4
Arg1+
4.44
CD45 (IV)
Arg1 (antiGFP)
cells/mono+mac (%)
cells/CD45iv- (%)
cells/CD45iv+ (%)
CD45iv-
CD45iv+
Arg1-
Arg1+
G
CD45iv-Arg1+/CD45iv+Arg1+
Normalized to Mode
Ly6c
p = 0.0047
Ly6c MFI
CD45iv- Arg1+
CD45iv+ Arg1+

Figure 3: Arg1^{+} macrophages are increased following *Hif1α* deletion, are derived from monocytes, and are specified prior to myocardial extravasation. A.) Control and *Cx3cr1^{creERT2}Hif1α$^{flox/flox}$* mice were treated with tamoxifen and harvested 4 days after MI. 20x confocal images of immunofluorescence staining within the infarct zone 4 days after MI. Arg1 (red) and macrophage marker CD68 (green). B.) *CCR2^{creERT2}Hif1α$^{flox/flox}$ Rosa26^{tdTomato}* mice were treated with a single dose of tamoxifen (60mg/kg) 1 day prior to MI to label infiltrating monocytes. 20x confocal images of immunofluorescence staining within the infarct zone of monocyte lineage labeled cells (tdTomato, white) costained with Arg1 (red) and the macrophage marker CD68 (green). C.) Quantification of the proportion of Arg1^{+} macrophages in A, data points represent the average of 5 20x fields per mouse. Data displays the percentage of Arg1^{+}CD68^{+} cells as a percentage of total CD68^{+} cells. D.) Quantification of tdTomato^{+}Arg1^{+} macrophages in B, data represents the average of 5 20x fields per mouse. Data displays the number of Arg1^{+}tdTomato^{+} cells and Arg1^{+}tdTomato^{-} cells as a percentage of total Arg1^{+}CD68^{+} cells. E.) Intravital 2-photon microscopy images of regions containing coronary veins of *Arg1^{YFP}* reporter mice 24 hours after syngeneic heart transplant, mice were imaged for a duration of 15 minutes. Arg1/YFP signal is in green, Q-dots (red) were injected intravascularly prior to imaging to visualize blood vessels. Collagen is in blue. Extravasated Arg1^{+} macrophages are green, intravascular Arg1^{+} cells crawling on the blood vessel wall co-stain are in yellow (highlighted by arrows). F.) Flow cytometry analysis of *Arg1^{YFP}* reporter mice 2 days after MI. Mice were injected with a CD45 antibody intravascularly 5 minutes prior to tissue collection (CD45iv). Flow panel included CD45, Ly6G, CD11b, Ly6C, CD64, CD45iv, and anti-GFP antibodies. CD45iv+ monocytes/macrophages were considered intravascular. CD45iv- monocytes/macrophages were considered extravascular. G.) Histogram of Ly6c staining between CD45iv-Arg1+ cells and CD45iv+Arg1+ cells vs cell counts normalized to mode. Quantification of Ly6c staining mean fluorescence intensity (MFI) between CD45iv-Arg1+ cells and CD45iv+Arg1+ cells. P-values are determined using a two tailed t-test assuming equal variance.

Figure 4:

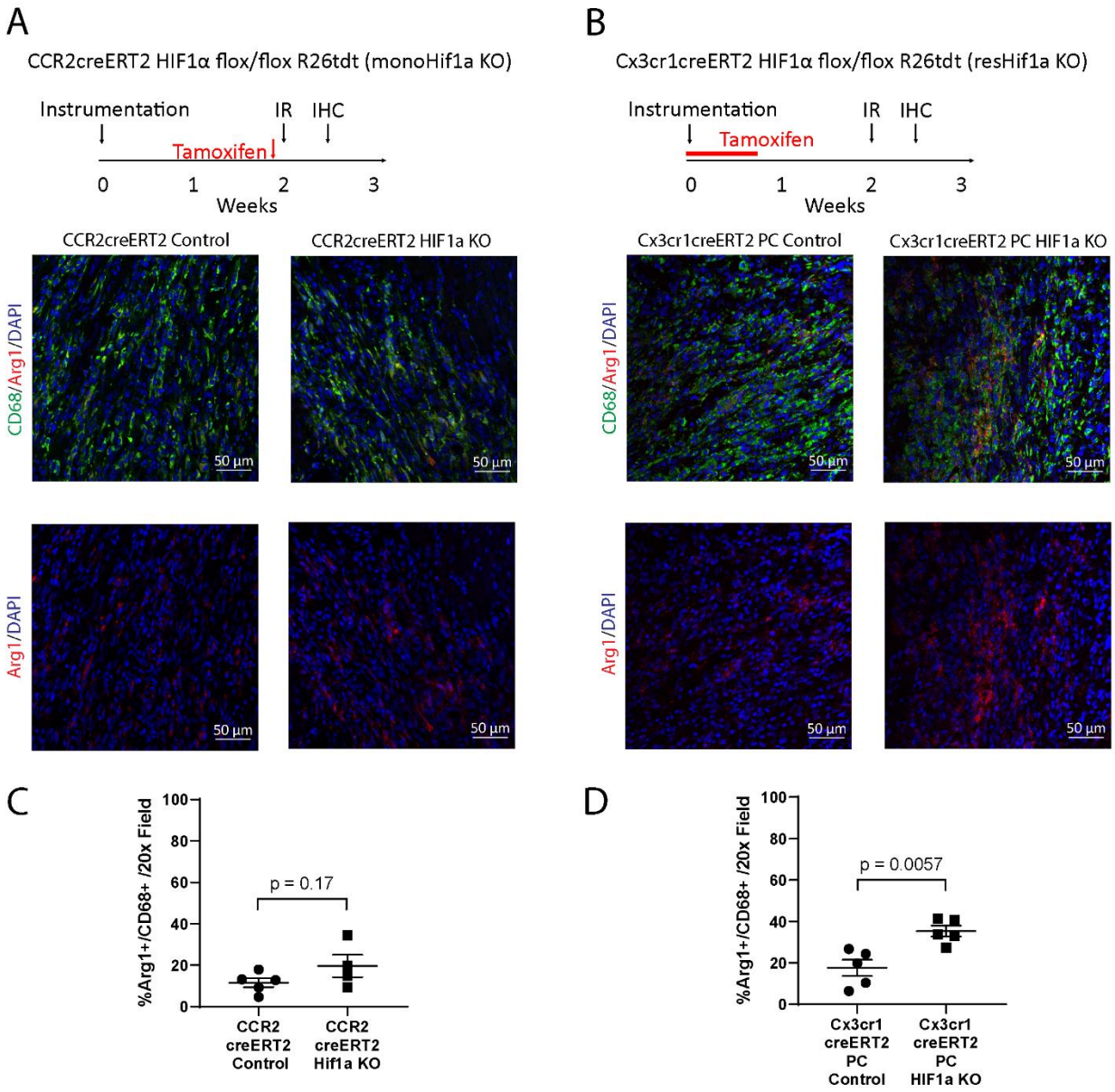
A
CCR2creERT2 HIF1α flox/flox R26tdt (monoHif1a KO)
Instrumentation
IR
IHC
Tamoxifen
0
1
2
3
Weeks
CCR2creERT2 Control
CCR2creERT2 HIF1a KO
CD68/Arg1/DAPI
Arg1/DAPI
50 µm
B
Cx3cr1creERT2 HIF1α flox/flox R26tdt (resHif1a KO)
Cx3cr1creERT2 PC Control
Cx3cr1creERT2 PC HIF1a KO
C
%Arg1+/CD68+ /20x Field
p = 0.17
CCR2 creERT2 Control
CCR2 creERT2 Hif1a KO
D
p = 0.0057
Cx3cr1 creERT2 PC Control
Cx3cr1 creERT2 PC HIF1a KO

Figure 4: *Hif1α* deletion in cardiac resident macrophages is sufficient to increase the abundance of Arg1^{+} macrophages. A.) 20x confocal images of immunofluorescence staining for Arg1 (red) and CD68 (green) in *CCR2^{creERT2}Hif1α$^{flox/flox}$* and control hearts treated with a single pulse of tamoxifen (60mg/kg) prior to MI. Immunostaining was performed 5 days following MI. B.) 20x confocal images of immunofluorescence staining for Arg1 (red) and CD68 (green) in *Cx3cr1^{creERT2}Hif1α$^{flox/flox}$* and control hearts. Mice were treated with pulse-chase tamoxifen to induce deletion in cardiac resident macrophages. Immunostaining was performed 4 days following MI. C.-D.) quantification of A and B, respectively. Data points represent the average of 5 20x fields per mouse. Data displays the percentage of Arg1^{+}CD68^{+} cells as a percentage of total CD68^{+} cells. P-values are determined using a two tailed t-test assuming equal variance.

Figure 5:

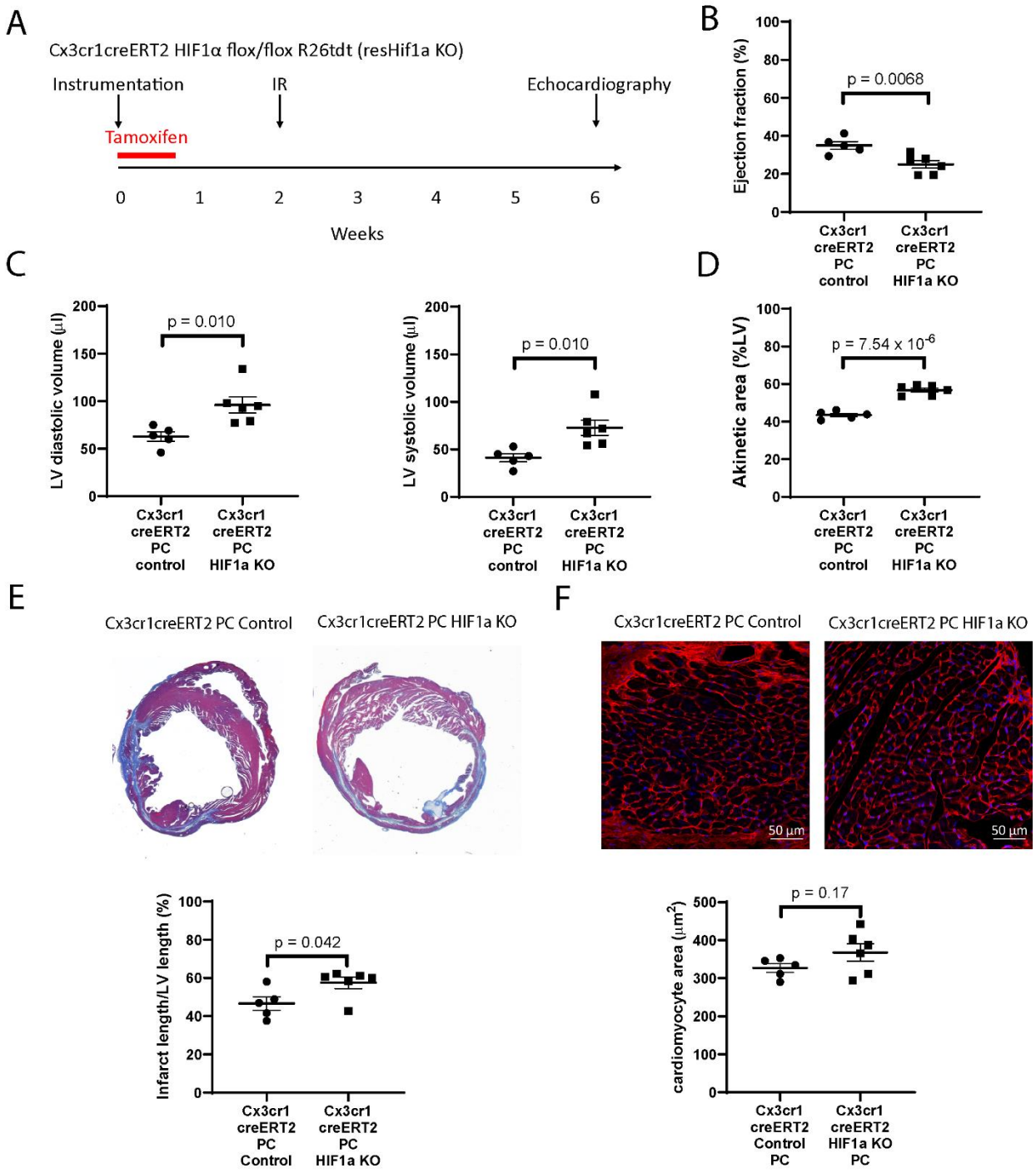
A
Cx3cr1creERT2 HIF1α flox/flox R26tdt (resHif1a KO)
Instrumentation
IR
Echocardiography
Tamoxifen
0
1
2
3
4
5
6
Weeks
B
Ejection fraction (%)
p = 0.0068
Cx3cr1 creERT2 PC control
Cx3cr1 creERT2 PC HIF1a KO
C
LV diastolic volume (µl)
p = 0.010
LV systolic volume (µl)
p = 0.010
D
Akinetic area (%LV)
p = 7.54 x 10-6
E
Cx3cr1creERT2 PC Control
Cx3cr1creERT2 PC HIF1a KO
Infarct length/LV length (%)
p = 0.042
Cx3cr1 creERT2 PC Control
Cx3cr1 creERT2 PC HIF1a KO
F
Cx3cr1creERT2 PC Control
Cx3cr1creERT2 PC HIF1a KO
50 µm
50 µm
cardiomyocyte area (µm2)
p = 0.17
Cx3cr1 creERT2 Control PC
Cx3cr1 creERT2 HIF1a KO PC

Figure 5: *Hif1α* deletion in cardiac resident macrophages is sufficient to increase infarct size, accelerate LV remodeling, and reduce LV systolic function after MI. A.) Experimental outline of closed chest ischemia reperfusion injury in *Cx3cr1*^{creERT2}*Hif1α*$^{flox/flox}$ mice treated with pulse-chase dosing of tamoxifen to delete *Hif1α* in cardiac resident macrophages. 5 daily injections of tamoxifen (60mg/kg) were administered after instrumentation. Mice were subjected to ischemia reperfusion injury after 9 days of normal chow diet. Echocardiography was performed 4 weeks after MI and hearts collected for analysis. B.) Echocardiographic quantification of ejection fraction in control and *Cx3cr1*^{creERT2}*Hif1α*$^{flox/flox}$ mice C.) Echocardiographic quantification of left ventricular diastolic volume and left ventricular systolic volume in control and *Cx3cr1*^{creERT2}*Hif1α*$^{flox/flox}$ mice. D.) Akinetic area as a percentage of left ventricle between Control and *Cx3cr1*^{creERT2}*Hif1α*$^{flox/flox}$ mice. E.) Trichrome staining and quantification of Control and *Cx3cr1*^{creERT2}*Hif1α*$^{flox/flox}$ hearts 4 weeks after MI. Data is displayed as the length of the infarct as a percentage of the total length of the left ventricle. F.) WGA staining of cardiomyocytes in the border zone 4 weeks after MI. Quantification of the average cardiomyocyte area in Control and *Cx3cr1*^{creERT2}*Hif1α*$^{flox/flox}$ hearts. Data points represent the average of 5 20x fields per mouse, with 12 cardiomyocytes selected at random per 20x field. P-values are determined using a two tailed t-test assuming equal variance.

References

1.) McMurray JJ, Pfeffer MA. Heart failure. Lancet. 2005 May 28-Jun 3;365(9474):1877-89. doi: 10.1016/S0140-6736(05)66621-4. PMID: 15924986.

2.) Roger VL. Epidemiology of heart failure. Circ Res. 2013 Aug 30;113(6):646-59. doi: 10.1161/CIRCRESAHA.113.300268. PMID: 23989710; PMCID: PMC3806290.

3.) Timmers L, Sluijter JP, van Keulen JK, Hoefer IE, Nederhoff MG, Goumans MJ, Doevendans PA, van Echteld CJ, Joles JA, Quax PH, Piek JJ, Pasterkamp G, de Kleijn DP. Toll-like receptor 4 mediates maladaptive left ventricular remodeling and impairs cardiac function after myocardial infarction. Circ Res. 2008 Feb 1;102(2):257-64. doi: 10.1161/CIRCRESAHA.107.158220. Epub 2007 Nov 15. PMID: 18007026.

4.) Lewis EF, Moye LA, Rouleau JL, Sacks FM, Arnold JM, Warnica JW, Flaker GC, Braunwald E, Pfeffer MA; CARE Study. Predictors of late development of heart failure in stable survivors of myocardial infarction: the CARE study. J Am Coll Cardiol. 2003 Oct 15;42(8):1446-53. doi: 10.1016/s0735-1097(03)01057-x. PMID: 14563590.

5.) Epelman S, Liu PP, Mann DL. Role of innate and adaptive immune mechanisms in cardiac injury and repair. Nat Rev Immunol. 2015 Feb;15(2):117-29. doi: 10.1038/nri3800. PMID: 25614321; PMCID: PMC4669103.

6.) Frantz S, Nahrendorf M. Cardiac macrophages and their role in ischaemic heart disease. Cardiovasc Res. 2014 May 1;102(2):240-8. doi: 10.1093/cvr/cvu025. Epub 2014 Feb 5. PMID: 24501331; PMCID: PMC3989449.

7.) Javaheri A, Bajpai G, Picataggi A, Mani S, Foroughi L, Evie H, Kovacs A, Weinheimer CJ, Hyrc K, Xiao Q, Ballabio A, Lee JM, Matkovich SJ, Razani B, Schilling JD, Lavine KJ, Diwan A. TFEB activation in macrophages attenuates postmyocardial infarction ventricular dysfunction independently of

ATG5- mediated autophagy. JCI Insight. 2019 Nov 1;4(21):e127312. doi: 10.1172/jci.insight.127312. PMID: 31672943; PMCID: PMC6948771.

8.) van Amerongen MJ, Harmsen MC, van Rooijen N, Petersen AH, van Luyn MJ. Macrophage depletion impairs wound healing and increases left ventricular remodeling after myocardial injury in mice. Am J Pathol. 2007 Mar;170(3):818-29. doi: 10.2353/ajpath.2007.060547. PMID: 17322368; PMCID: PMC1864893.

9.) Kaikita K, Hayasaki T, Okuma T, Kuziel WA, Ogawa H, Takeya M. Targeted deletion of CC chemokine receptor 2 attenuates left ventricular remodeling after experimental myocardial infarction. Am J Pathol. 2004 Aug;165(2):439-47. doi: 10.1016/S0002-9440(10)63309-3. PMID: 15277218; PMCID: PMC1618584.

10.) Bajpai G, Bredemeyer A, Li W, Zaitsev K, Koenig AL, Lokshina I, Mohan J, Ivey B, Hsiao HM, Weinheimer C, Kovacs A, Epelman S, Artyomov M, Kreisel D, Lavine KJ. Tissue Resident CCR2- and CCR2+ Cardiac Macrophages Differentially Orchestrate Monocyte Recruitment and Fate Specification Following Myocardial Injury. Circ Res. 2019 Jan 18;124(2):263-278. doi: 10.1161/CIRCRESAHA.118.314028. PMID: 30582448; PMCID: PMC6626616.

11.) Bajpai G, Schneider C, Wong N, Bredemeyer A, Hulsmans M, Nahrendorf M, Epelman S, Kreisel D, Liu Y, Itoh A, Shankar TS, Selzman CH, Drakos SG, Lavine KJ. The human heart contains distinct macrophage subsets with divergent origins and functions. Nat Med. 2018 Aug;24(8):1234-1245. doi: 10.1038/s41591-018-0059-x. Epub 2018 Jun 11. PMID: 29892064; PMCID: PMC6082687.

12.) Lavine KJ, Epelman S, Uchida K, Weber KJ, Nichols CG, Schilling JD, Ornitz DM, Randolph GJ, Mann DL. Distinct macrophage lineages contribute to disparate patterns of cardiac recovery and remodeling in the neonatal and adult heart. Proc Natl Acad Sci U S A. 2014 Nov 11;111(45):16029-34. doi: 10.1073/pnas.1406508111. Epub 2014 Oct 27. Erratum in: Proc Natl Acad Sci U S A. 2016 Mar 8;113(10):E1414. Dosage error in article text. PMID: 25349429; PMCID: PMC4234568.

13.) Wang GL, Jiang BH, Rue EA, Semenza GL. Hypoxia-inducible factor 1 is a basic-helix-loop-helix-PAS heterodimer regulated by cellular O2 tension. Proc Natl Acad Sci U S A. 1995 Jun 6;92(12):5510-4. doi: 10.1073/pnas.92.12.5510. PMID: 7539918; PMCID: PMC41725.

14.) Semenza GL, Wang GL. A nuclear factor induced by hypoxia via de novo protein synthesis binds to the human erythropoietin gene enhancer at a site required for transcriptional activation. Mol Cell Biol. 1992 Dec;12(12):5447-54. doi: 10.1128/mcb.12.12.5447-5454.1992. PMID: 1448077; PMCID: PMC360482.

15.) Wang GL, Semenza GL. General involvement of hypoxia-inducible factor 1 in transcriptional response to hypoxia. Proc Natl Acad Sci U S A. 1993 May 1;90(9):4304-8. doi: 10.1073/pnas.90.9.4304. PMID: 8387214; PMCID: PMC46495.

16.) Yona S, Kim KW, Wolf Y, Mildner A, Varol D, Breker M, Strauss-Ayali D, Viukov S, Guilliams M, Misharin A, Hume DA, Perlman H, Malissen B, Zelzer E, Jung S. Fate mapping reveals origins and dynamics of monocytes and tissue macrophages under homeostasis. Immunity. 2013 Jan 24;38(1):79-91. doi: 10.1016/j.immuni.2012.12.001. Epub 2012 Dec 27. Erratum in: Immunity. 2013 May 23;38(5):1073-9. PMID: 23273845; PMCID: PMC3908543.

17.) Ryan HE, Poloni M, McNulty W, Elson D, Gassmann M, Arbeit JM, Johnson RS. Hypoxia-inducible factor-1alpha is a positive factor in solid tumor growth. Cancer Res. 2000 Aug 1;60(15):4010-5. PMID: 10945599.

18.) Madisen L, Zwingman TA, Sunkin SM, Oh SW, Zariwala HA, Gu H, Ng LL, Palmiter RD, Hawrylycz MJ, Jones AR, Lein ES, Zeng H. A robust and high-throughput Cre reporting and characterization system for the whole mouse brain. Nat Neurosci. 2010 Jan;13(1):133-40. doi: 10.1038/nn.2467. Epub 2009 Dec 20. PMID: 20023653; PMCID: PMC2840225.

19.) Croxford AL, Lanzinger M, Hartmann FJ, Schreiner B, Mair F, Pelczar P, Clausen BE, Jung S, Greter M, Becher B. The Cytokine GM-CSF Drives the Inflammatory Signature of CCR2+ Monocytes and

Licenses Autoimmunity. Immunity. 2015 Sep 15;43(3):502-14. doi: 10.1016/j.immuni.2015.08.010. Epub 2015 Sep 1. PMID: 26341401.

20.) Reese TA, Liang HE, Tager AM, Luster AD, Van Rooijen N, Voehringer D, Locksley RM. Chitin induces accumulation in tissue of innate immune cells associated with allergy. Nature. 2007 May 3;447(7140):92-6. doi: 10.1038/nature05746. Epub 2007 Apr 22. PMID: 17450126; PMCID: PMC2527589.

21.) Hao Y, Hao S, Andersen-Nissen E, Mauck WM 3rd, Zheng S, Butler A, Lee MJ, Wilk AJ, Darby C, Zager M, Hoffman P, Stoeckius M, Papalexi E, Mimitou EP, Jain J, Srivastava A, Stuart T, Fleming LM, Yeung B, Rogers AJ, McElrath JM, Blish CA, Gottardo R, Smibert P, Satija R. Integrated analysis of multimodal single-cell data. Cell. 2021 Jun 24;184(13):3573-3587.e29. doi: 10.1016/j.cell.2021.04.048. Epub 2021 May 31. PMID: 34062119; PMCID: PMC8238499.

22.) Lavine KJ, Pinto AR, Epelman S, Kopecky BJ, Clemente-Casares X, Godwin J, Rosenthal N, Kovacic JC. The Macrophage in Cardiac Homeostasis and Disease: JACC Macrophage in CVD Series (Part 4). J Am Coll Cardiol. 2018 Oct 30;72(18):2213-2230. doi: 10.1016/j.jacc.2018.08.2149. PMID: 30360829; PMCID: PMC6209119.

23.) Stuart T, Butler A, Hoffman P, Hafemeister C, Papalexi E, Mauck WM 3rd, Hao Y, Stoeckius M, Smibert P, Satija R. Comprehensive Integration of Single-Cell Data. Cell. 2019 Jun 13;177(7):1888-1902.e21. doi: 10.1016/j.cell.2019.05.031. Epub 2019 Jun 6. PMID: 31178118; PMCID: PMC6687398.

24.) Love MI, Huber W, Anders S. Moderated estimation of fold change and dispersion for RNA-seq data with DESeq2. Genome Biol. 2014;15(12):550. doi: 10.1186/s13059-014-0550-8. PMID: 25516281; PMCID: PMC4302049.

25.) Chen EY, Tan CM, Kou Y, Duan Q, Wang Z, Meirelles GV, Clark NR, Ma'ayan A. Enrichr: interactive and collaborative HTML5 gene list enrichment analysis tool. BMC Bioinformatics. 2013 Apr 15;14:128. doi: 10.1186/1471-2105-14-128. PMID: 23586463; PMCID: PMC3637064.

26.) Kuleshov MV, Jones MR, Rouillard AD, Fernandez NF, Duan Q, Wang Z, Koplev S, Jenkins SL, Jagodnik KM, Lachmann A, McDermott MG, Monteiro CD, Gundersen GW, Ma'ayan A. Enrichr: a comprehensive gene set enrichment analysis web server 2016 update. Nucleic Acids Res. 2016 Jul 8;44(W1):W90-7. doi: 10.1093/nar/gkw377. Epub 2016 May 3. PMID: 27141961; PMCID: PMC4987924.

27.) Xie Z, Bailey A, Kuleshov MV, Clarke DJB, Evangelista JE, Jenkins SL, Lachmann A, Wojciechowicz ML, Kropiwnicki E, Jagodnik KM, Jeon M, Ma'ayan A. Gene Set Knowledge Discovery with Enrichr. Curr Protoc. 2021 Mar;1(3):e90. doi: 10.1002/cpz1.90. PMID: 33780170; PMCID: PMC8152575.

28.) Pico AR, Kelder T, van Iersel MP, Hanspers K, Conklin BR, Evelo C. WikiPathways: pathway editing for the people. PLoS Biol. 2008 Jul 22;6(7):e184. doi: 10.1371/journal.pbio.0060184. PMID: 18651794; PMCID: PMC2475545.

29.) Lachmann A, Xu H, Krishnan J, Berger SI, Mazloom AR, Ma'ayan A. ChEA: transcription factor regulation inferred from integrating genome-wide ChIP-X experiments. Bioinformatics. 2010 Oct 1;26(19):2438-44. doi: 10.1093/bioinformatics/btq466. Epub 2010 Aug 13. PMID: 20709693; PMCID: PMC2944209.

30.) Setty M, Kiseliovas V, Levine J, Gayoso A, Mazutis L, Pe'er D. Characterization of cell fate probabilities in single-cell data with Palantir. Nat Biotechnol. 2019 Apr;37(4):451-460. doi: 10.1038/s41587-019-0068-4. Epub 2019 Mar 21. Erratum in: Nat Biotechnol. 2019 Oct;37(10):1237. PMID: 30899105; PMCID: PMC7549125.

31.) Semenza GL. HIF-1 and human disease: one highly involved factor. Genes Dev. 2000 Aug 15;14(16):1983-91. PMID: 10950862.

32.) Lavine KJ, Sintek M, Novak E, Ewald G, Geltman E, Joseph S, Pfeifer J, Mann DL. Coronary collaterals predict improved survival and allograft function in patients with coronary allograft vasculopathy. Circ Heart Fail. 2013 Jul;6(4):773-84. doi: 10.1161/CIRCHEARTFAILURE.113.000277. Epub 2013 May 24. PMID: 23709657; PMCID: PMC3863089.

33.) Swirski FK, Nahrendorf M. Cardioimmunology: the immune system in cardiac homeostasis and disease. Nat Rev Immunol. 2018 Dec;18(12):733-744. doi: 10.1038/s41577-018-0065-8. PMID: 30228378.

34.) Dick SA, Macklin JA, Nejat S, Momen A, Clemente-Casares X, Althagafi MG, Chen J, Kantores C, Hosseinzadeh S, Aronoff L, Wong A, Zaman R, Barbu I, Besla R, Lavine KJ, Razani B, Ginhoux F, Husain M, Cybulsky MI, Robbins CS, Epelman S. Self-renewing resident cardiac macrophages limit adverse remodeling following myocardial infarction. Nat Immunol. 2019 Jan;20(1):29-39. doi: 10.1038/s41590-018-0272-2. Epub 2018 Dec 11. Erratum in: Nat Immunol. 2019 Mar 12;: PMID: 30538339; PMCID: PMC6565365.

35.) Glass CK, Saijo K. Nuclear receptor transrepression pathways that regulate inflammation in macrophages and T cells. Nat Rev Immunol. 2010 May;10(5):365-76. doi: 10.1038/nri2748. PMID: 20414208.

36.) Kobayashi EH, Suzuki T, Funayama R, Nagashima T, Hayashi M, Sekine H, Tanaka N, Moriguchi T, Motohashi H, Nakayama K, Yamamoto M. Nrf2 suppresses macrophage inflammatory response by blocking proinflammatory cytokine transcription. Nat Commun. 2016 May 23;7:11624. doi: 10.1038/ncomms11624. PMID: 27211851; PMCID: PMC4879264.

37.) Gilchrist M, Thorsson V, Li B, Rust AG, Korb M, Roach JC, Kennedy K, Hai T, Bolouri H, Aderem A. Systems biology approaches identify ATF3 as a negative regulator of Toll-like receptor 4. Nature. 2006 May 11;441(7090):173-8. doi: 10.1038/nature04768. Erratum in: Nature. 2008 Feb 21;451(7181):1022. Roach, Jared C [added]. PMID: 16688168.

38.) Hull RP, Srivastava PK, D'Souza Z, Atanur SS, Mechta-Grigoriou F, Game L, Petretto E, Cook HT, Aitman TJ, Behmoaras J. Combined ChIP-Seq and transcriptome analysis identifies AP-1/JunD as a primary regulator of oxidative stress and IL-1β synthesis in macrophages. BMC Genomics. 2013 Feb 11;14:92. doi: 10.1186/1471-2164-14-92. PMID: 23398888; PMCID: PMC3608227.

39.) Dorrington MG, Fraser IDC. NF-κB Signaling in Macrophages: Dynamics, Crosstalk, and Signal Integration. Front Immunol. 2019 Apr 9;10:705. doi: 10.3389/fimmu.2019.00705. PMID: 31024544; PMCID: PMC6465568.

40.) Epelman S, Lavine KJ, Beaudin AE, Sojka DK, Carrero JA, Calderon B, Brija T, Gautier EL, Ivanov S, Satpathy AT, Schilling JD, Schwendener R, Sergin I, Razani B, Forsberg EC, Yokoyama WM, Unanue ER, Colonna M, Randolph GJ, Mann DL. Embryonic and adult-derived resident cardiac macrophages are maintained through distinct mechanisms at steady state and during inflammation. Immunity. 2014 Jan 16;40(1):91-104. doi: 10.1016/j.immuni.2013.11.019. PMID: 24439267; PMCID: PMC3923301.

41.) Naresh NK, Xu Y, Klibanov AL, Vandsburger MH, Meyer CH, Leor J, Kramer CM, French BA, Epstein FH. Monocyte and/or macrophage infiltration of heart after myocardial infarction: MR imaging by using T1-shortening liposomes. Radiology. 2012 Aug;264(2):428-35. doi: 10.1148/radiol.12111863. Epub 2012 Jun 21. PMID: 22723500; PMCID: PMC3401349.

42.) Aronoff L, Epelman S, Clemente-Casares X. Isolation and Identification of Extravascular Immune Cells of the Heart. J Vis Exp. 2018 Aug 23;(138):58114. doi: 10.3791/58114. PMID: 30199044; PMCID: PMC6231712.

43.) Abe H, Takeda N, Isagawa T, Semba H, Nishimura S, Morioka MS, Nakagama Y, Sato T, Soma K, Koyama K, Wake M, Katoh M, Asagiri M, Neugent ML, Kim JW, Stockmann C, Yonezawa T, Inuzuka R, Hirota Y, Maemura K, Yamashita T, Otsu K, Manabe I, Nagai R, Komuro I. Macrophage hypoxia

signaling regulates cardiac fibrosis via Oncostatin M. Nat Commun. 2019 Jun 27;10(1):2824. doi: 10.1038/s41467-019-10859-w. PMID: 31249305; PMCID: PMC6597788.

44.) DeBerge M, Lantz C, Dehn S, Sullivan DP, van der Laan AM, Niessen HWM, Flanagan ME, Brat DJ, Feinstein MJ, Kaushal S, Wilsbacher LD, Thorp EB. Hypoxia-inducible factors individually facilitate inflammatory myeloid metabolism and inefficient cardiac repair. J Exp Med. 2021 Sep 6;218(9):e20200667. doi: 10.1084/jem.20200667. Epub 2021 Jul 29. PMID: 34325467; PMCID: PMC8329871.

45.) Clausen BE, Burkhardt C, Reith W, Renkawitz R, Förster I. Conditional gene targeting in macrophages and granulocytes using LysMcre mice. Transgenic Res. 1999 Aug;8(4):265-77. doi: 10.1023/a:1008942828960. PMID: 10621974.

46.) Wang J, Seo MJ, Deci MB, Weil BR, Canty JM, Nguyen J. Effect of CCR2 inhibitor-loaded lipid micelles on inflammatory cell migration and cardiac function after myocardial infarction. Int J Nanomedicine. 2018 Oct 15;13:6441-6451. doi: 10.2147/IJN.S178650. PMID: 30410330; PMCID: PMC6198873.

47.) Gardner PJ, Liyanage SE, Cristante E, Sampson RD, Dick AD, Ali RR, Bainbridge JW. Hypoxia inducible factors are dispensable for myeloid cell migration into the inflamed mouse eye. Sci Rep. 2017 Jan 23;7:40830. doi: 10.1038/srep40830. PMID: 28112274; PMCID: PMC5256030.

48.) Nahrendorf M, Swirski FK, Aikawa E, Stangenberg L, Wurdinger T, Figueiredo JL, Libby P, Weissleder R, Pittet MJ. The healing myocardium sequentially mobilizes two monocyte subsets with divergent and complementary functions. J Exp Med. 2007 Nov 26;204(12):3037-47. doi: 10.1084/jem.20070885. Epub 2007 Nov 19. PMID: 18025128; PMCID: PMC2118517.

49.) Viola A, Munari F, Sánchez-Rodríguez R, Scolaro T, Castegna A. The Metabolic Signature of Macrophage Responses. Front Immunol. 2019 Jul 3;10:1462. doi: 10.3389/fimmu.2019.01462. PMID: 31333642; PMCID: PMC6618143.

50.) Yang Z, Ming XF. Functions of arginase isoforms in macrophage inflammatory responses: impact on cardiovascular diseases and metabolic disorders. Front Immunol. 2014 Oct 27;5:533. doi: 10.3389/fimmu.2014.00533. PMID: 25386179; PMCID: PMC4209887.

51.) Mouton AJ, DeLeon-Pennell KY, Rivera Gonzalez OJ, Flynn ER, Freeman TC, Saucerman JJ, Garrett MR, Ma Y, Harmancey R, Lindsey ML. Mapping macrophage polarization over the myocardial infarction time continuum. Basic Res Cardiol. 2018 Jun 4;113(4):26. doi: 10.1007/s00395-018-0686-x. PMID: 29868933; PMCID: PMC5986831.

52.) Schindelin J, Arganda-Carreras I, Frise E, Kaynig V, Longair M, Pietzsch T, Preibisch S, Rueden C, Saalfeld S, Schmid B, Tinevez JY, White DJ, Hartenstein V, Eliceiri K, Tomancak P, Cardona A. Fiji: an open-source platform for biological-image analysis. Nat Methods. 2012 Jun 28;9(7):676-82. doi: 10.1038/nmeth.2019. PMID: 22743772; PMCID: PMC3855844.

53.) Li W, Hsiao HM, Higashikubo R, Saunders BT, Bharat A, Goldstein DR, Krupnick AS, Gelman AE, Lavine KJ, Kreisel D. Heart-resident CCR2+ macrophages promote neutrophil extravasation through TLR9/MyD88/CXCL5 signaling. JCI Insight. 2016 Aug 4;1(12):e87315. doi: 10.1172/jci.insight.87315. PMID: 27536731; PMCID: PMC4985028.